Multistage cyclotron autoresonance accelerator

Changbiao Wang and J. L. Hirshfield
Physics Department, Yale University, New Haven, Connecticut 06520-1820
and Omega-P Incorporated, 202008 Yale Station, New Haven, Connecticut 06520
(Received 24 September 1997; revised manuscript received 19 February 1998)

It has been shown previously that a cyclotron autoresonance accelerator (CARA) has a practical upper energy limit that arises from axial velocity stalling in the rising axial magnetic field. This paper shows that this upper energy limit can be overcome by operating a series of CARA stages, with each succeeding stage at a higher gyroharmonic. The accelerator would be driven from a single external rf source, and gyroharmonic operation in stages beyond the first would be accomplished by stagewise reduction in the guide magnetic field. Analytical and simulation results are presented to show, under ideal conditions, that stalling can thereby be avoided and acceleration to high energy can be achieved. For a three-stage CARA with a 15-A, 250-kV injected electron beam driven by 75 MW of rf power at 11.424 GHz, the results show that an energy of over 5 MeV can be reached at the end of the third stage, whereas a practical single-stage CARA with a 250-kV injected beam has an upper energy limit of about 1.7 MeV. It is also shown that tandem operation of a large number of CARA stages could, in principle, allow acceleration of electrons up to GeV energies.
[S1063-651X(98)14906-1]

PACS number(s): 29.17.+w, 29.27.−a, 41.75.−i, 52.75.Ms

I. INTRODUCTION

Cyclotron autoresonance acceleration (CARA) of electrons [1–11] has received attention in recent years because of its potential for preparing an energetic gyrating beam for use in gyroharmonic generators of rf power [3,7–11], and for efficient preparation of a megavolt beam that may find industrial application in pollution remediation and materials processing [12]. It has been demonstrated experimentally that CARA can efficiently accelerate an electron beam with an rf-to-beam power efficiency of up to 96% [1]. But a significant property of CARA is that acceleration is limited: There exists an upper energy limit that depends on the injected energy and on the final guided wave refractive index, assuming that rf beam loading does not impose a lower limit. The upper energy limit arises since the transverse component of applied magnetic field increases with increase of beam energy, thus reducing the electron's axial velocity towards stalling [3–5].

This paper describes a way in which this upper energy limit can be circumvented by operating a multistage CARA. Successive stages would operate at successively higher gyroharmonics, but at the same frequency. This requires an adiabatic reduction in the guide magnetic field between one stage and the next, thereby increasing the axial momentum of the electrons, and avoiding stalling. However, in contrast to a single-stage CARA, which produces a continuous (unbunched) beam, a multistage version can only accelerate a bunched beam synchronized in phase at each stage. The calculations and simulation results presented in this paper are for a zero-emittance ideally bunched beam, in order to illustrate the principles of multistage CARA operation. Clearly, any reduction to practice must be preceded by more detailed analysis that takes into account the finite emittance of the beam, and that optimizes injection conditions at each stage to maximize phase stability; such considerations are beyond the scope of this paper.

In a single-stage CARA electrons are injected along the axis of a cylindrical TE_{11} mode waveguide immersed in an axially varying static magnetic field. Microwave power with a frequency of ω is fed at the input end of the waveguide to drive a rotating mode, and the axial magnetic field $B_0(z)$ is adjusted along the waveguide axis z to maintain resonance, approximately satisfying the relation $B_0(z)=(m_0\omega/e)\gamma(z)[1-n(z)\beta_z(z)]$, where m_0 and e are the electron rest mass and charge, $\gamma(z)$ is the electron Lorentz energy factor, $n(z)$ is the guided wave refractive index, and $\beta_z(z)$ is the electron axial velocity normalized to the speed of light.

The upper energy limit $\gamma_{\rm lim}$ for a single-stage CARA has been previously found to be

$$\gamma_{\rm lim}=\gamma_0^*+\left[\frac{(\gamma_0^{*2}-1)}{(1-n_f^2)}\right]^{1/2}. \tag{1}$$

Here γ_0^* is the effective initial electron energy factor, and $n_f=ck_{zf}/\omega$ is the refractive index at the end of CARA, with c the speed of light, and k_{zf} the axial wave number at the end of the accelerator. For convenience to the reader, this relationship is rederived in Appendix A. The effective initial energy factor is given by $\gamma_0^*=\gamma_0\xi$, where γ_0 is the initial electron energy factor itself, and ξ is an energy reduction coefficient defined as $\xi=1-0.5\beta_{\perp 0}^2/(1-n_0\beta_{z0})$, with $\beta_{\perp 0}$ and β_{z0} the initial transverse and axial velocities normalized to c, and n_0 the refractive index at the beginning of CARA. The initial and final refractive indices n_0 and n_f differ when a tapered waveguide is employed. The energy reduction coefficient ξ depends only on parameters at the entrance of CARA, and ranges from $0.5(1+1/\gamma_0^2)$ for zero initial axial velocity, to unity for zero initial transverse velocity. For a given initial beam energy, a beam with larger transverse velocity has a smaller axial velocity and is more susceptible to stalling. The energy reduction coefficient ξ is seen to decrease with increasing initial transverse velocity. As an ex-

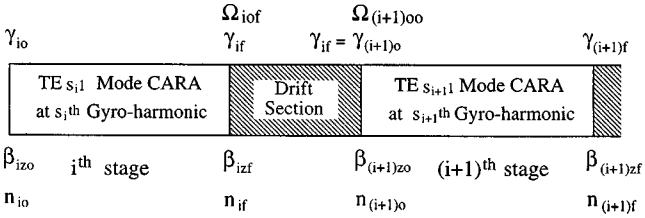

FIG. 1. Diagram of a multistage cyclotron autoresonance accelerator. In the drift section between the ith and $(i+1)$th stages, there is a mode converter.

ample, if one takes in Eq. (1) $\gamma_0^*=1.4892$ (250 kV) and $n_f=0.9262$ or 0.9741 (corresponding to a 2.04-cm or 3.40-cm radius TE_{11} mode waveguide at 11.424 GHz), one finds $\gamma_{\rm lim}=4.4168$ or 6.3685 (1.75 or 2.74 MV).

It can be seen from Eq. (1) that the upper energy limit increases with an increase in both waveguide refractive index and effective initial energy. Accordingly, there are two ways to increase the upper energy limit. One is to increase the refractive index by increasing or up-tapering the waveguide radius, as in the 3.40-cm radius example above. Unfortunately this will give rise to a rapid decrease in accelerating gradient, and an excessive increase in length of the accelerating structure. The other approach is to increase the effective initial energy, a strategy that also has practical limits. An alternative approach would be to inject the accelerated beam from one CARA into a second CARA for further acceleration, and so on. This paper examines a means for achieving this and thereby increasing this upper energy limit by the use of several stages of CARA in tandem.

II. THEORY OF A MULTISTAGE CARA

In contrast to the situation for a single-stage CARA, use of a multistage CARA may allow one to obtain a higher acceleration energy within a reasonable structure length, by operating subsequent CARA stages at the same frequency, but at increasing gyroharmonics. The axial magnetic field beyond the end of one stage must be reduced to allow gyroharmonic resonance at the beginning of the next stage. This decrease in axial magnetic field B_0 causes an increase in β_z, thus avoiding stalling. rf power can be injected from an external source (e.g., a high power klystron or magnicon) into the first stage, thence directly into subsequent stages in sequence with in-line waveguide mode converters between stages. The mode converters are to allow CARA interactions at the mth gyroharmonic through coupling to the TE_{m1} mode of the cylindrical waveguide, according to the established selection rule for gyroharmonic interactions with axis-encircling orbits [8,13–15].

Figure 1 shows a diagram of the ith and $(i+1)$th stages of a multistage CARA. The ith stage operates in the TE_{s_i1} mode at the s_ith gyroharmonic and the $(i+1)$th stage operates in the $TE_{s_{i+1}1}$ mode at the s_{i+1}th gyroharmonic. Between the two stages there is a drift section where TE_{s_i1} mode rf power remaining at the end of the ith stage flows into the $TE_{s_{i+1}1}$ mode through a mode converter, and the axial magnetic field is reduced to match resonance with the s_{i+1}th gyroharmonic. The first stage operates in the TE_{11} mode at the fundamental in order to accelerate an injected pencil beam. If, at the end of the ith stage the electron beam reaches its upper energy limit, and if no interaction takes place in the drift section, a derivation is presented in Appendix B, which shows the effective initial energy of the $(i+1)$th stage to be expressible in terms of that of the s_ith stage. That is,

$$\gamma^*_{(i+1)0}=\gamma^*_{i0}+\left(1-\frac{s_i}{s_{i+1}}\right)\left(\frac{\gamma^{*2}_{i0}-1}{1-n^2_{if}}\right)^{1/2}. \tag{2}$$

And the $(i+1)$th stage acceleration energy is given using Eq. (1), i.e.,

$$\gamma_{(i+1)f}=\gamma^*_{(i+1)0}+\left[\frac{\gamma^{*2}_{(i+1)0}-1}{1-n^2_{(i+1)f}}\right]^{1/2}. \tag{3}$$

These results assume that either sufficiently high rf power is injected, or sufficiently low beam current is employed, so that rf power depletion does not limit the acceleration energy.

From Eq. (2) it can be seen that if the harmonic index increases successively stage by stage, then the effective initial energy of each stage goes up as well. Equations (2) and (3) can be used to find algebraic estimates for the acceleration energy of a multistage CARA. We take as an example a three-stage CARA with an initial electron beam energy of 250 kV. The harmonic indices chosen for the three stages are $s_1=1$, $s_2=3$, and $s_3=5$, and the refractive indices are $n_{1f}=0.9262$, $n_{2f}=0.6927$, and $n_{3f}=0.6156$, respectively. For the first stage, since $\xi_1=1$ (zero initial transverse velocity), and $\gamma^*_{10}=\gamma_{10}=1.4892$ (250 kV), we have $\gamma_{1f}=4.4168$ from Eq. (3) with $i=0$. For the second stage, we have $\gamma^*_{20}=3.4410$ and $\gamma_{2f}=8.0061$, respectively, from Eqs. (2) and (3) with $i=1$; and for the third stage, $\gamma^*_{30}=5.2670$ and $\gamma_{3f}=11.8287$ again from Eqs. (2) and (3) with $i=2$. The choice of waveguide radii that led to the refractive indices used will be justified below. This simple example shows acceleration from 250 kV to 5.53 MV in a three-stage CARA. This can be compared with a final energy of 1.75 MV that obtains from Eq. (1) for a 2.04-cm radius waveguide single-stage CARA, i.e., $n_{1f}=0.9262$.

In Appendix C it is shown that, in the cyclotron autoresonance interaction, the normalized electron's gyration radius satisfies the inequality

$$\frac{r_L}{R_w}<\frac{s}{j'_{s1}}<1, \tag{4}$$

where r_L is the gyration radius, R_w is the waveguide radius, s is the harmonic index, and j'_{s1} is the first root of the derivative of the Bessel function $J_s(\chi)$. For example, r_L/R_w is less than 0.5431 for the TE_{11} mode CARA, less than 0.7141 for the TE_{31} mode CARA, and less than 0.7793 for the TE_{51} mode CARA. This shows that, in each stage, the beam would be reasonably separated from the waveguide wall.

In Appendix D it is shown that the initial waveguide radius for the $(i+1)$th stage, which results from use of the resonance conditions, the adiabatic condition, and with $s_iB_{i0f}=s_{i+1}B_{(i+1)00}$, can be found to be

$$R_{w(i+1)0}=\frac{\lambda_0 j'_{s_{i+1}1}}{2\pi}\times\left[\frac{\beta_{izf}^2+(1-s_i/s_{i+1})\beta_{i\perp f}^2}{(1-n_{if}^2)\beta_{izf}^2+(1-s_i/s_{i+1})\beta_{i\perp f}^2}\right]^{1/2}. \quad (5)$$

where λ_0 is the rf free-space wavelength. An example is given below showing use of the above formula. Suppose that the first stage operates in the TE_{11} mode at 11.424 GHz at the fundamental gyroharmonic with a final waveguide radius R_{w1f} of 2.04 cm, and that the second stage operates in the TE_{31} mode at the third gyroharmonic. Given the normalized transverse and axial velocities at the end of the first stage to be 0.7154 and 0.6580, respectively; then inserting these values and $\lambda_0=2.6242$ cm (11.424 GHz), $s_1=1$, $s_2=3$, $j'_{31}=4.201\,189$, and $n_{1f}=0.9262$ into Eq. (5) with $i=1$ we obtain the initial waveguide radius for the second stage $R_{w20}=2.43$ cm.

Phase matching between the accelerated beam and the rf field is an important issue when the beam enters a following stage. Therefore, it is worthwhile giving a general discussion about the phase relation between two electromagnetic waves that interact synchronously with the same beam, and then apply it to the case of a multistage CARA. Suppose that an electron beam is synchronous with the electromagnetic wave with a rf frequency of ω_i and an axial wave number of k_{iz} in the ith interaction region. For all the electrons having the same guiding center, the electron and wave phases at any interaction cross section are related by the approximate conservation equation

$$\psi_i(z,t)-(m_i-s_i)\theta_g(z,t)-s_i\phi(z,t)=C_i \quad (z_{i0}\leqslant z\leqslant z_{if}), \quad (6)$$

where $\psi_i(z,t)=\omega_i t-\int k_{iz}dz$ is the wave phase, m_i is the azimuthal mode index, $\theta_g(z,t)$ is the guiding-center azimuthal coordinate, $\phi(z,t)$ is the electron's gyration angle, C_i is a constant in the sense that $\partial C_i/\partial t=0$ and $\partial C_i/\partial z=0$, and z_{i0} and z_{if} are, respectively, the beginning and the end of the ith interaction region. In the drift section where resonance is not satisfied and coupling between the particles and fields is weak, Eq. (6) should not be expected to hold.

It should be stressed that Eq. (6) is not an exact constant of motion because it assumes slow variations, neglects refractive effects and velocity and energy spreads of the beam, and assumes that pump depletion is small. The velocity and energy spreads during acceleration of particles to higher energies are the main source of phase deviation from resonance because in such a situation only one particle, in principle, can be set in exact resonance by adjusting the applied magnetic field. The order of approximation made in Eq. (6) is the same as that in Eq. (1). Single particle simulations for the example presented below in this paper indicate that the right-hand side of Eq. (6) changes within a range of less than 3°.

Dividing the both sides of Eq. (6) by s_i, we have

$$\frac{\psi_i(z,t)}{s_i}-\left(\frac{m_i}{s_i}-1\right)\theta_g(z,t)-\phi(z,t)=\frac{C_i}{s_i} \quad (z_{i0}\leqslant z\leqslant z_{if}). \quad (7)$$

Applying Eq. (7) to the end of the ith region and the beginning of the $(i+1)$th region and taking their difference with the assumption

$$\frac{m_i}{s_i}=\frac{m_{i+1}}{s_{i+1}}, \quad (8)$$

we obtain

$$\left[\frac{\psi_{i+1}(z_{(i+1)0},t)}{s_{i+1}}-\frac{\psi_i(z_{if},t)}{s_i}\right]=\frac{C_{i+1}}{s_{i+1}}-\frac{C_i}{s_i}+\left(\frac{m_i}{s_i}-1\right)\Delta\theta_g+\Delta\phi, \quad (9)$$

where

$$\Delta\theta_g\equiv\theta_g(z_{(i+1)0},t)-\theta_g(z_{if},t) \quad (10)$$

and

$$\Delta\phi\equiv\phi(z_{(i+1)0},t)-\phi(z_{if},t).$$

In the above, $\Delta\theta_g$ and $\Delta\phi$ are increments of the guiding center angle θ_g and gyration angle ϕ when the electron goes through the drift section. Assuming that no interaction exists in the drift section allows one to take $\partial[(m_i/s_i-1)\Delta\theta_g+\Delta\phi]/\partial t=0$. Considering that the phase difference for the same wave between any two cross sections is independent of time, that is, $\partial(\Delta\psi_i)/\partial t=0$, from Eq. (9) we have

$$\frac{\partial}{\partial t}\left[\frac{\psi_{i+1}(z_{i+1},t)}{s_{i+1}}-\frac{\psi_i(z_i,t)}{s_i}\right]=0 \quad (11)$$

or

$$\frac{\psi_{i+1}(z_{i+1},t)}{s_{i+1}}-\frac{\psi_i(z_i,t)}{s_i}=\text{const},$$

where z_i and z_{i+1} represent any cross section in the ith and $(i+1)$th regions, and the constant depends on locations of the cross sections. Equations (8) and (11), which are generalized from the cogeneration conditions [16], indicate that the phase is fixed between two waves that interact synchronously with the same beam. Letting ψ_i and ψ_{i+1} denote phases of two different waves in the same stage, while z_i and z_{i+1} denote the same location, we obtain the phase-locking equation for the cogeneration case where the two waves with the same ratio of azimuthal mode index to harmonic index $(m_i/s_i=1)$ interact synchronously with the beam in the same waveguide [10]. In the case that has been demonstrated experimentally [17], where $s_1=1$, $s_2=2$, $m_1=2$, and $m_2=4$ with $m_1/s_1=m_2/s_2$ automatically fulfilled, and $\omega_1/s_1=\omega_2/s_2$, Eq. (11) with $i=1$ becomes $\psi_2(z_2,t)/s_2-\psi_1(z_1,t)/s_1=-\int^{z_2}k_{2z}dz+\int^{z_1}k_{1z}dz$, a time-independent constant.

In the multistage CARA configuration where $m_i/s_i=1$ and $\omega_i=\omega_{i+1}=2\pi c/\lambda_0$, Eq. (8) is fulfilled, and thus Eqs. (9) and (11) hold although $\omega_i/s_i\neq\omega_{i+1}/s_{i+1}$. The axial component of the magnetic field in the drift section varies slowly enough so that the adiabatic condition $\beta_\perp^2/B_0=\text{const}$ is satisfied. The electron's gyration angle increment

$\Delta\phi$ appearing in Eq. (9) is adjustable by changing the magnetic field profile within the drift section, without causing a deviation from the resonance condition $\omega - k_z\beta_z c - s\Omega_0/\gamma = 0$ at the ends of the adjacent interaction regions. Here the nonrelativistic gyration frequency is defined by $\Omega_0 = eB_0/m_0$ with e and m_0 the electron charge and rest mass, respectively. Accordingly, the accelerated beam keeps interacting synchronously with the rf fields in the next stage CARA if a proper magnetic field profile is imposed.

III. SIMULATION ANALYSIS FOR A THREE-STAGE CARA

Single-particle simulations have been carried out for a three-stage single-frequency CARA with the first TE_{11} stage operating at the fundamental, the second TE_{31} stage at the third gyroharmonic, and the third TE_{51} stage at the fifth gyroharmonic. This single-particle model corresponds to an ideally bunched electron beam. Between stages, 30-cm-long drift sections are inserted that contain mode converters. In this example, a 15-A, 250-kV injected electron beam is assumed, driven at the injector end by 75 MW of rf power at 11.424 GHz. The single-stage CARA code [3] was used to run the three-stage device stage by stage, by assuming that the particle is exactly synchronous at optimum phase with the rf fields at the beginning of the second and the third stages. The rf power is fed from the beginning of the first stage, and it is assumed that the leftover power from the first and second stages, respectively, is completely converted into the power of TE_{31} and TE_{51} modes through the mode converters in the intervening drift sections. In the first stage, the waveguide has three segments: the first segment has a radius of 0.96 cm and a length of 5.0 cm, the third segment has a radius of 2.04 cm and a length of 4.0 cm; the second segment is tapered between them with a length of 10 cm. This arrangement of different waveguide radii is to allow a larger acceleration energy within a shorter acceleration length than for a constant radius. Calculation shows less than 1% power conversion from TE_{11} mode to TM_{11} mode in the tapered section [18]. The 0.96-cm radius waveguide can only support the TE_{11} mode; it has a larger accelerating gradient but a lower upper energy limit, as compared with 2.04-cm radius. Introduction of the taper is to avoid beam stalling and hence to increase the acceleration energy. Equation (5) was used to calculate waveguide radii for the second and third stages. For the second stage, the waveguide is uniform with a radius of 2.43 cm and a length of 68 cm; for the third stage, the waveguide with a length of 115 cm is tapered up from 3.02 to 3.4 cm. Deviation of waveguide radius from the design value will cause the electron beam to deviate from its resonance condition, and the beam acceleration energy to decrease with an increase in deviation. By using different radii and comparing acceleration energies using simulations, it is found that Eq. (5) is well confirmed.

Figure 2 shows the dependence of beam energy and rf power on axial distance, from simulation for the three stage CARA. In the first stage (from $z=0$ to 19 cm), 75-MW rf power at TE_{11} mode is injected to drive the 250-kV beam, and 21.3480 MW is absorbed, with a remaining power of 53.6520 MW flowing into the TE_{31} mode through the TE_{11}-TE_{31} mode converter in the 30-cm drift section [18].

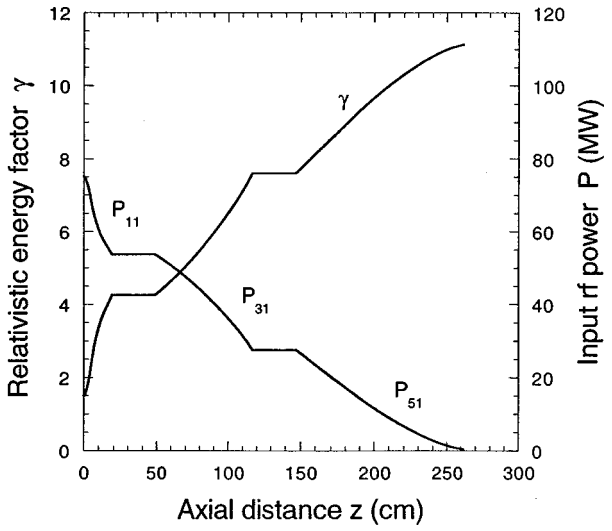

FIG. 2. Dependence of beam energy and rf power on axial distance. P_{11}, P_{31}, and P_{51} denote TE_{11}, TE_{31}, and TE_{51} powers, respectively. 98.5% of 75 MW rf power at 11.424 GHz is converted into beam power and the beam is accelerated from 250 kV to 5.17 MV.

The relativistic energy factor γ is increased to 4.2552 (1.6634 MV), compared with the analytically calculated value 4.4168. The difference comes mainly from the fact that the beam should not be accelerated right up to its upper energy limit to avoid beam stalling. In the second stage (from $z=49$ to 117 cm), TE_{31} mode power is decreased to 27.5629 MW, all flowing into the third stage TE_{51} mode through the mode converter in the second drift section; the acceleration energy is increased to $\gamma=7.6091$ (3.3773 MV), compared with the analytic value 8.0061. In the third stage (from $z=147$ to 262 cm), TE_{51} mode power is decreased to 0.3384 MW; the acceleration energy is increased to $\gamma = 11.1237$ (5.1732 MV), compared with the analytic value 11.8287. The total rf conversion efficiency for the three-stage CARA is 98.5%, corresponding to a beam power of 77.5982 MW. The wall loss due to finite conductivity ($\sigma = 5.56\times10^7$ Siemens/m for copper) is 0.1466 MW for the first stage, 0.3815 MW for the second, and 0.2851 MW for the third, with the effect of wall taper taken into account. Inefficiency is thus dominated by wall losses, which account in total for 0.8132 MW, while the spent beam accounts for only 0.3386 MW. For a finite-emittance beam, power in the spent beam can be expected to be larger.

Figure 3 shows the dependence of axial velocity and axial magnetic field on axial distance. At the first stage end ($z = 19$ cm), the axial velocity β_z is decreased to 0.6580 after two gentle oscillations, and the axial magnetic field B_0 is increased to 6.7825 kG. If the beam were to continue to be accelerated using the fundamental TE_{11} mode, the axial magnetic field growth rate would become intolerably large because of the rapid decrease in axial velocity and increase in beam energy, so that an excessively strong transverse magnetic field arises and beam stalling results. Thus a drift section is used wherein the transverse magnetic field can be reduced to the value needed for acceleration in the next stage. In the first drift section, the axial magnetic field B_0 is reduced to 2.2608 kG, and the axial velocity β_z is increased

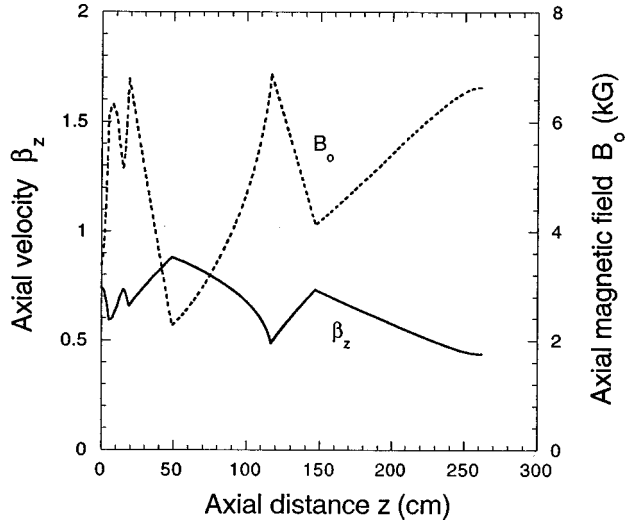

FIG. 3. Dependence of axial velocity and magnetic field on axial distance. In the drift section, the axial magnetic field is decreased and axial velocity is increased to reduce transverse magnetic field and avoid beam stalling while matching the resonance condition for the next stage CARA.

to 0.8798, the transverse velocity $\beta_\perp$ is reduced from 0.7154 to 0.4132, matching the resonance condition for the second stage. The increase in axial velocity and the decrease in beam energy growth rate (resulting from the decrease in transverse velocity) greatly reduce the transverse magnetic field to avoid beam stalling, and then the second stage continues to accelerate the beam with a higher effective initial energy. At the end of second stage ($z=117$ cm), the axial velocity β_z is decreased to 0.4861 and the axial magnetic field B_0 is increased to 6.8660 kG. Again, the axial magnetic field B_0 is reduced to 4.1196 kG and the axial velocity β_z is increased to 0.7303 in the drift section to match the resonance condition for the third stage. In the third stage, β_z is decreased to 0.4381 and B_0 is increased to 6.6309 kG during acceleration. The sharp magnetic field peaks shown in Fig. 3 may not be realizable in practice, but experience with a single-stage tapered CARA [1] has shown that effects of deviation from such field profiles can be compensated by mild detuning of the field nearby.

It is found in the simulation that the maximum normalized gyration radius $(r_L/R_w)_{\max}$ is 0.4689 in the first stage, 0.6983 in the second, and 0.7737 in the third. These values are consistent with the analytic predictions from Eq. (4), which are given by $r_L/R_w<0.5431$ for the first, 0.7141 for the second, and 0.7793 for the third.

IV. HIGH-ENERGY MULTISTAGE CARA

The results presented in Sec. III could be the basis for a more detailed analysis including effects of finite initial beam emittance, realizable magnetic field profiles, and actual fields in the mode converters. This analysis could lead to design and construction of a 5-MeV, 75-MW high average power accelerator that could find applications in advanced gyroharmonic radiation sources, or in electron beam processing. But it may be that a CARA with many stages could lead to acceleration to much higher energies, in which case the range of applications would increase. Thus, it may be worthwhile

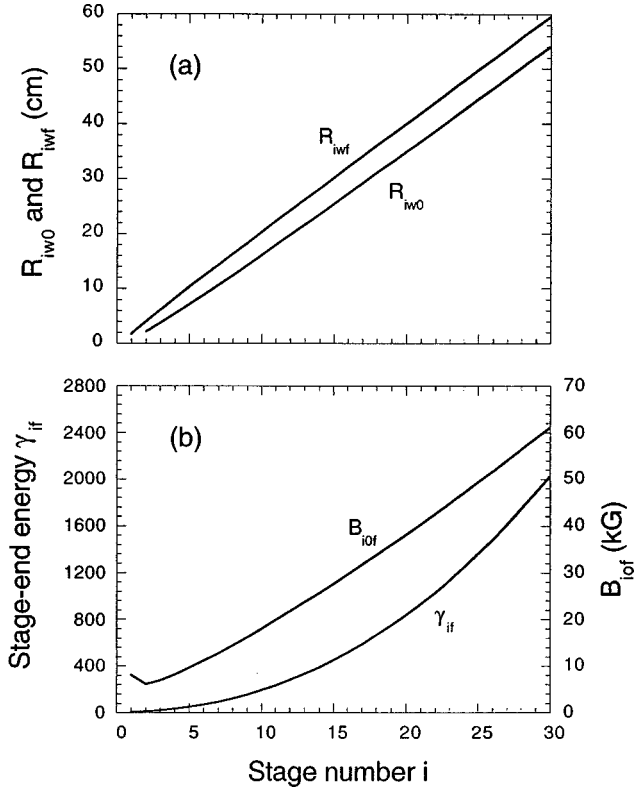

FIG. 4. Dependence of (a) initial waveguide radius R_{iw0} and final waveguide radius R_{iwf}, and (b) resulting energy factor γ_{if} and stage-end magnetic field B_{i0f} on stage number i. The azimuthal mode index is $s_i=2i-1$ for the ith stage.

to indicate what the iterative use of Eqs. (2), (3), and (5) can predict for the ultimate energy that could, in principle, be reached when the number of stages becomes large. To illustrate, it is assumed that a 250-kV beam is injected into the first TE_{11}-mode stage, that subsequent stages have odd azimuthal mode indices, and that the final refractive index of each stage is 0.90. Figure 4 shows the resulting energy factor, the magnetic field at the end of each stage, and the initial and final waveguide radii for each stage, all as functions of stage number i; the azimuthal mode index is $s_i=2i-1$. It is seen that acceleration to a energy of over 1 GeV is predicted after 30 stages, with an outer radius of the final $TE_{59,1}$ waveguide equal to 60 cm and the axial magnetic field equal to 61 kG. Synchrotron radiation from such a beam would undoubtedly be a significant factor. It can be remarked that a 1-GeV beam cycling in a 61-kG magnetic field has a critical photon energy in its synchrotron radiation spectrum of greater than 4 keV. This calculation demonstrates only what could in principle be possible with a multistage CARA having many stages; whether such a machine could in practice be built can only be answered after significant further analysis, design, and testing.

V. CONCLUSIONS

This paper has described a multistage CARA configuration that permits acceleration to energies higher than what can be achieved in a single stage. Operation at successively higher gyroharmonics allows the axial magnetic field to decrease between stages, thus avoiding stalling. A three-stage

CARA is analyzed in detail. Single-particle simulation results are in agreement with analytical predictions. The ideal single-particle model, which assumed an ideally bunched beam, was used in the analysis to understanding the potential for a multi-stage CARA, although clearly a practical beam will have finite emittance. Generally speaking, higher harmonic CARAs require a better beam quality, and the gyrophase spread in a sth harmonic CARA should be at least less than π/s for efficient acceleration. Further analysis is needed to assess the influence of finite initial beam emittance, realizable magnetic field profiles, and possible interactions in the mode converters. It is important to investigate means for stabilizing particle gyrophases during acceleration, i.e., to achieve good phase trapping, for lessening the sensitivity of operation to finite beam emittance and to the precision of the practical magnetic field profile. Preliminary results show that a 15-A, 250-kV electron beam driven by 75 MW of rf power at 11.424 GHz can be accelerated to 5.17 MeV, in an overall length (including waveguide mode converters) of slightly over 2.5 m. The maximum axial magnetic field is less than 7 kG. The rf-to-beam power transfer efficiency is found to be 98.5%, assuming ideal mode conversion. A single-stage CARA with similar parameters would have an upper energy limit of 1.75 MeV, for a 2.04-cm waveguide radius, or 2.74 MV for a 3.4-cm waveguide radius. High average power 1–5-MeV electron beams have numerous practical applications, including in radiation sources, for pollution remediation, and for materials processing.

Operation of a CARA with many stages is also discussed, insofar as finding an estimate of the ultimate electron energy that can be achieved in principle. It is found that an energy of over 1 GeV could be reached in a 30-stage CARA. Since this device would require a magnetic field rising to over 60 kG at its end, it is possible that a novel light source would result, with a critical synchrotron radiation photon energy, which scales as $\gamma^2 B_0$, that exceeds 4 keV. Clearly, further analysis is required before it is known whether construction of such a high-energy machine is practical.

ACKNOWLEDGMENTS

Appreciation is extended to D. F. Sutter for suggesting a study of the multistage CARA. This work was supported by Department of Energy, Divisions of High Energy Physics and Advanced Energy Projects.

APPENDIX A: DERIVATION OF EQ. (1)

During CARA acceleration, the axial velocity β_z, the electron energy factor γ, and the refractive index n at any point along the accelerator are related by the resonance condition and approximate constant of motion [3], which are, respectively, given by

$$s\Omega_0/\omega=\gamma(1-n\beta_z), \tag{A1}$$

$$\frac{(\gamma\beta_\perp)^2}{(s\Omega_0/\omega)}-2\gamma=\text{const}, \tag{A2}$$

where s is the harmonic index and $\Omega_0=eB_0/m_0$ is the nonrelativistic gyration frequency, with B_0 the axial magnetic field, e and m_0 the electron charge and rest mass, respectively.

Inserting Eq. (A1) into Eq. (A2) and taking the initial values for the constant, we obtain

$$\frac{(\gamma\beta_\perp)^2}{\gamma(1-n\beta_z)}-2\gamma=-2\gamma_0\left(1-\frac{\beta_{\perp 0}^2}{2(1-n_0\beta_{z0})}\right), \tag{A3}$$

or

$$\frac{(\gamma\beta_\perp)^2}{\gamma(1-n\beta_z)}-2(\gamma-\gamma_0^*)=0. \tag{A4}$$

Considering $\beta_\perp^2=1-1/\gamma^2-\beta_z^2$ and solving Eq. (A4) for β_z, we obtain

$$\beta_z=\frac{1}{\gamma}\left[n(\gamma-\gamma_0^*)+D^{1/2}\right], \tag{A5}$$

where $D=n^2(\gamma-\gamma_0^*)^2-(\gamma^2-2\gamma\gamma_0^*+1)$. Since $D\geqslant 0$ we have

$$\gamma\leqslant\gamma_0^*+\left[\frac{(\gamma_0^{*2}-1)}{(1-n^2)}\right]^{1/2}. \tag{A6}$$

Setting the waveguide index n equal to n_f at the end of CARA, we obtain Eq. (1).

APPENDIX B: DERIVATION OF EQ. (2)

The effective initial energy factor for the $(i+1)$st stage CARA is defined by

$$\gamma_{(i+1)0}^*=\gamma_{(i+1)0}\xi_{i+1}=\gamma_{if}\xi_{i+1}, \tag{B1}$$

where $\gamma_{if}=\gamma_{(i+1)0}$, no energy loss in the drift section is taken into account, and the corresponding energy reduction coefficient is given by

$$\xi_{i+1}=1-\frac{\beta_{(i+1)\perp 0}^2}{2(1-n_{(i+1)0}\beta_{(i+1)z0})}. \tag{B2}$$

Applying the adiabatic condition to the two ends of the ith drift section (see Fig. 1), we have

$$\frac{\gamma_{if}^2\beta_{i\perp f}^2}{\Omega_{i0f}}=\frac{\gamma_{(i+1)0}^2\beta_{(i+1)\perp 0}^2}{\Omega_{(i+1)00}} \quad \text{or} \quad \beta_{(i+1)\perp 0}^2=\frac{\Omega_{(i+1)00}}{\Omega_{i0f}}\,\beta_{i\perp f}^2. \tag{B3}$$

The resonance conditions at the two ends can be written as

$$1-n_{if}\beta_{izf}=s_i\Omega_{i0f}/\omega, \tag{B4}$$

$$1-n_{(i+1)0}\beta_{(i+1)z0}=s_{i+1}\Omega_{(i+1)00}/\omega. \tag{B5}$$

Combining the above two equations, we obtain

$$1-n_{(i+1)0}\beta_{(i+1)z0}=(1-n_{if}\beta_{izf})\,\frac{s_{i+1}\Omega_{(i+1)00}}{s_i\Omega_{i0f}}. \tag{B6}$$

From the approximate constant of motion given by Eq. (A4), we have

$$\frac{\beta_{i\perp f}^2}{(1-n_{if}\beta_{izf})}=2\left(1-\frac{\gamma_{i0}^*}{\gamma_{if}}\right). \tag{B7}$$

Inserting Eqs. (B3) and (B6) into Eq. (B2) with the help of Eq. (B7) yields

$$\xi_{i+1}=1-\frac{1}{2}\frac{s_i}{s_{i+1}}\frac{\beta_{i\perp f}^2}{(1-n_{if}\beta_{izf})}=1-\frac{s_i}{s_{i+1}}\left(1-\frac{\gamma_{i0}^*}{\gamma_{if}}\right). \tag{B8}$$

Substituting Eq. (B8) into Eq. (B1), we have

$$\gamma_{(i+1)0}^*=\gamma_{if}-\frac{s_i}{s_{i+1}}(\gamma_{if}-\gamma_{i0}^*). \tag{B9}$$

We have assumed that at the end of each stage the electron beam gets its upper energy limit described by Eq. (A6), that is,

$$\gamma_{if}=\gamma_{i0}^*+\left[\frac{(\gamma_{i0}^{*2}-1)}{(1-n_{if}^2)}\right]^{1/2}. \tag{B10}$$

Finally, substituting the above expression into Eq. (B9), we obtain the recurrence formula Eq. (2) for effective initial energy factor.

APPENDIX C: DERIVATION OF EQ. (4)

Assuming that the resonance condition is always satisfied during acceleration, the gyration radius, defined by $\gamma\beta_\perp c/\Omega_0$, can be written from Eq. (A1) as

$$r_L=\frac{c}{\omega}\frac{s\alpha\beta}{(1+\alpha)^{1/2}-n\beta}, \tag{C1}$$

where $\alpha=\beta_\perp/\beta_z$ and $\beta=(1-1/\gamma^2)^{1/2}$.

The waveguide radius for TE_{ml} mode is given by

$$R_w=\frac{c}{\omega}\frac{j'_{ml}}{(1-n^2)^{1/2}}, \tag{C2}$$

where j'_{ml} is the lth root of the derivative of the Bessel function $J_m(\chi)$.

Comparing Eq. (C1) and Eq. (C2), we obtain

$$\frac{r_L}{R_w}=\frac{s}{j'_{ml}}\frac{\alpha\beta(1-n^2)^{1/2}}{(1+\alpha)^{1/2}-n\beta}\leqslant\frac{s\beta}{j'_{ml}}\left(\frac{1-n^2}{1-n^2\beta^2}\right)^{1/2}<\frac{s\beta}{j'_{ml}}<\frac{s}{j'_{ml}}. \tag{C3}$$

In the CARA, $m=s\geqslant 1$ and $l=1$ are usually used, and according to property of Bessel function [19] we know $s<j'_{s1}$. From this we obtain Eq. (4).

APPENDIX D: DERIVATION OF EQ. (5)

From Eq. (C2), we have the initial waveguide radius for the $(i+1)$th stage

$$R_{(i+1)w0}=\frac{c}{\omega}\frac{j'_{s_{i+1}1}}{(1-n_{(i+1)0}^2)^{1/2}}. \tag{D1}$$

Assuming $s_i\Omega_{i0f}=s_{i+1}\Omega_{(i+1)00}$, from Eq. (B6) and Eq. (B3) we have

$$n_{(i+1)0}=\frac{n_{if}\beta_{izf}}{\beta_{(i+1)z0}}, \tag{D2}$$

$$\beta_{(i+1)\perp 0}^2=\frac{s_i}{s_{i+1}}\beta_{i\perp f}^2. \tag{D3}$$

From Eq. (D3) we have

$$\beta_{(i+1)z0}=(1-1/\gamma_{(i+1)0}^2-\beta_{(i+1)\perp 0}^2)^{1/2}=\left[\beta_{izf}^2+\left(1-\frac{s_i}{s_{i+1}}\right)\beta_{i\perp f}^2\right]^{1/2}. \tag{D4}$$

Inserting Eq. (D4) into Eq. (D2) and then the resultant Eq. (D2) into Eq. (D1), we obtain Eq. (5).

[1] M. A. LaPointe, R. B. Yoder, C. Wang, A. K. Ganguly, and J. L. Hirshfield, Phys. Rev. Lett. **76**, 2718 (1996).

[2] J. L. Hirshfield, M. A. LaPointe, A. K. Ganguly, R. B. Yoder, and C. Wang, Phys. Plasmas **3**, 2163 (1996).

[3] C. Wang and J. L. Hirshfield, Phys. Rev. E **51**, 2456 (1995).

[4] B. Hafizi, P. Sprangle, and Hirshfield, Phys. Rev. E **50**, 3077 (1994).

[5] C. Chen, Phys. Fluids B **3**, 2933 (1991); Phys. Rev. A **46**, 6654 (1992).

[6] L. Friedland, Phys. Plasmas **1**, 421 (1994).

[7] A. J. Balkcum, D. B. McDermott, K. C. Leou, F. V. Hartmann, and N. C. Luhmann, Jr., IEEE Trans. Plasma Sci. **22**, 913 (1994).

[8] A. K. Ganguly and J. L. Hirshfield, Phys. Rev. E **47**, 4364 (1993).

[9] J. L. Hirshfield, C. Wang, and A. K. Ganguly, IEEE Trans. Plasma Sci. **24**, 825 (1996).

[10] C. Wang, J. L. Hirshfield, and A. K. Ganguly, Phys. Rev. Lett. **77**, 3819 (1996).

[11] J. L. Hirshfield, C. Wang, and A. K. Ganguly (unpublished).

[12] K. Whitham, Bull. Am. Phys. Soc. **42**, 1391 (1997).

[13] J. Y. Choe and S. Ahn, IEEE Trans. Electron Dev. **28**, 94 (1981).

[14] P. Vitello and K. Ko, IEEE Trans. Plasma Sci. **13**, 454 (1985).

[15] G. Nusinovich, Int. J. Electron. **72**, 959 (1992).

[16] J. L. Hirshfield and C. Wang (unpublished).

[17] H. Guo, S. H. Chen, V. L. Granatstein, J. Rodgers, G. Nusinovich, M. Walter, B. Levush, and W. J. Chen, Phys. Rev. Lett. **79**, 515 (1997).

[18] M. Shapiro (private communications).

[19] F. W. J. Olver, in *Handbook of Mathematical Functions with Formulas, Graphs, and Mathematical Tables*, edited by M. Abramowitz and I. A. Stegun (Dover Publications, New York, 1972), p. 370.